AEROELASTIC CONTROL BY FUZZY LOGIC OF A LINEAR FLEXIBLE WING WITH EMBEDDED PIEZOELECTRIC ACTUATORS

Edson Mulero Gruppioni, grupioni@sc.usp.br
Flavio Donizeti Marques, fmarques@sc.usp.br
Engineering School of São Carlos / University of São Paulo EESC/USP 13566-590 – São Carlos – SP – Brazil

Abstract. *Aeronautical structures are submitted to a variety of aeroelastic phenomena that may compromise its performance. With the development of new materials, aeronautical structures have becoming lighter, flexible, and they have being more subjected to aeroelastic problems, such as flutter and buffeting. Researchers have been worked on alternatives to solve these undesired aeroelastic problems, as the recent concept of smart or intelligent structures. Smart structures are those that present embedded sensors and actuators in the structure, integrated with control systems and signal processing, to enable the adaptation of the structural system to changes in the operational conditions. Mathematical models that incorporate actuator elements or sensors are of great importance in preliminary analysis of smart aeronautical structures. In this context, modeling methods are necessary to capture structural dynamic behavior and unsteady aerodynamic loading. The objective of this work is the study of an active fuzzy controller for aeroelastic response of a smart wing with embedded piezoelectric actuators. Linear characteristics of aeroelastic responses will be analised for critical flutter conditions. The finite elements method for the linear structural model and vortex-lattice method for the unsteady aerodynamic model has been used.*

Keywords: *aeroelasticity, active control, smart structure, smart wing, piezoelectric actuator*

1. INTRODUCTION

Aeronautical structures are subjected to many sources of excitations, mainly due to aerodynamic flow interactions, that lead to disturbances and vibrations. With the current requirements for lighter aircraft and the development of new materials, aeronautical structures are becoming more flexible, and being more subject to aeroelastic problems, such as flutter, buffeting and limit cycle oscillations. Other sources can affect the aeroelastic system, like strain displacement or geometric non-linearities, dry friction, shock wave motions, and separated flows (Dowell and Tang, 2002). Another class of aircraft, like high altitude long endurance, specifically unmanned aerial vehicles (UAV's) (Cesnick and Brown, 2002; Patil et al., 2001), and vehicles with morphing wings (Forster and Livne, 2000; Gern et al., 2001), have been studied to enhance flight performance and less surface controls. These aircraft need specific control strategies mainly because of non-linear effects (aerodynamics and structural dynamics) and complex actuation system.

In this context, developments on numerical solutions for aeroelastic models to be used for aircraft design purpose have become very important and have received special attention from the scientific community. The numerical models for aeroelastic analysis can be divided in two vast categories, which are: ones in the frequency domain and in the time domain. The frequency domain based solutions are the classical ones, but are valid only in the stability boundary, i.e., they can only be employed for predicting critical aeroelastic conditions. The time domain based solutions allow the determination of the aeroelastic response time history for any flight condition, and they have the additional advantage of allowing the inclusion of non-linear effects and the design of control systems for vibration suppression.

A great amount of research has been done to solve aeroelastic control problems, with application of active and passive solutions to the structure. Recently, expressive developments on the use of active materials incorporated into the structures have been done. Piezoelectric materials have been the most used ones for sensors and actuators devices, as well as optic fibers, shape memory alloys, and electro- and magneto-rheological fluids and gels. With the purpose of modifying the form or position, integrating active elements into the structures together with a control system, signal processing, and electronic systems, the concept of Smart Structure or Intelligent Structure (IS) has been defined (Crawley, 1994). An important aspect in the development of IS is the control system. Due to increasingly systems complexity, the non-conventional control techniques have been explored in the design of non-linear controllers and/or in the operation of complex environments with uncertainties and ambiguous parameters. Non-conventional techniques are those that do not follow the classic and modern control techniques approach. Here they comprise the artificial neural networks (ANN) (Haykin, 1999) and fuzzy logic (FL) (Yager and Filev, 1994).

This work presents an active aeroelastic control strategy for vibration suppression of a flexible smart wing based on fuzzy logic. The finite element method (FEM) has been used to model the wing structure, which has been assumed with embedded piezoelectric actuators (Marques and Nagamine, 2001). The vortex-lattice method (VLM) has been used for the unsteady aerodynamic model (Benini et al, 2001). Both structural and aerodynamic models have been treated separately and the information exchange between the aerodynamic and structural meshes has been done by a surface spline interpolation scheme (Benini, 2002). The control methodology has been based on Mamdani-type FL control, to aim vibration suppression on the wing tip, following the procedure by Gruppioni (2002) and Nagamine (2001). The FL

controller has been emulated by an ANN, which interpolates the decision surface on pre-determined universe of discourse. The following sections present structural and aerodynamic models, the FL controller design methodology, and the results achieved for a hypothetical wing model.

2. MATHEMATICAL MODELING

This section will treat the mathematical modeling of a smart flexible with the structural model approached by finite element method, considering the Kirchhoff plate element assumptions.

2.1 Smart wing description

The flexible wing here can be approached by a cantilever beam, therefore the aerodynamic model treats the wing as plain plate. The dimensions of the wing are $0.8 \times 0.25m$ of semi-span and chord, respectively, wich are the length and width of the main structure. The piezoelectric actuators then are bonded along the semi-span, as shown in Fig. 1, always at pairs (in top and under of the main structure).

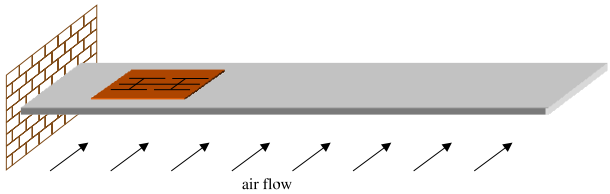

Figure 1. Schematic of the flexible smart wing structure.

2.2 Modal transformation

The wing structural response is assumed to be linear and without internal damping. The equation of motion for the structure is shown in Eq. (1), where M and K are the mass and stiffness matrices, and $\{x(t)\}$, $\{\ddot{x}(t)\}$ and $\{L(\{x\},\{\ddot{x}\},t)\}$ are the vectors, representing the displacements, accelerations and external mechanical, electric and aerodynamic loadings.

$$[M]\{\ddot{x}(t)\} + [K]\{x(t)\} = \{L(\{x\},\{\ddot{x}\},t)\} \tag{1}$$

The mode shapes can be arranged in a matrix according to

$$[\Phi] = [\ \{\varphi_1\} \quad \{\varphi_2\} \quad \{\varphi_3\} \quad \cdots \quad \{\varphi_N\}\ ] \tag{2}$$

that is named modal matrix and is used as a coordinate transformation matrix, that is:

$$\{x(t)\} = [\Phi]\{\eta(t)\} = \sum_{r=1}^{N} \psi_r \eta_r(t) \tag{3}$$

where $\{\eta(t)\}$ represents the structural displacements in a modal domain and can be interpreted as a vector of coefficients which determines the influence of each mode shape in the physical structural response (Meirovitch, 1986).

Since the vector $\{\eta\}$ is constant with time, it follows that:

$$\{\ddot{x}(t)\} = [\Phi]\{\ddot{\eta}(t)\} \tag{4}$$

Substituting Eqs. (3) and (4) in Eq. (1) and pre-multiplying both sides by $[\Phi]^T$,

$$[M_m]\{\ddot{\eta}(t)\} + [K_m]\{\eta(t)\} = [\Phi]^T\{L(\{x\},\{\ddot{x}\},t)]\} \tag{5}$$

where $[M_m] = [\Phi]^T[M][\Phi]$ and $[K_m] = [\Phi]^T[K][\Phi]$ are named modal mass and modal stiffness matrices, respectively.

Due to the orthogonality properties of the mode shapes, one can prove that the matrices $[M_m]$ and $[K_m]$ are diagonal matrices. In addition, it is possible to normalize the eingenvectors in a form that $[M_m] = [I]$, and then the division of both sides of Eq. (5) by the matrix $[M_m]$,

$$\{\ddot{\eta}(t)\} + [\omega^2]\{\eta(t)\} = [\Phi]^T\{L(\{x\},\{\ddot{x}\},t)\} \tag{6}$$

where $[\omega^2]$ is a diagonal matrix containing the squared natural frequencies.

In order to simplify the solution of Eq. (6), it is useful to consider only a few natural modes to describe the structural response. This is done by truncating the summation in Eq. (3). In fact, only a few modes are necessary to obtain a solution with good precision (Meirovitch, 1986).

2.3 Model of the active structure

From the principle of Hamilton electro-mechanical variational principle can be assessed. The FEM has been used to model an active plate, representative for the wing structure. Piezoelectric behavior has been also incorporated to the model.

2.3.1 Electro-mechanical behavior

From Hamilton's principle, it follows:

$$\delta \int_{t_1}^{t_2} (T-U)\mathrm{d}t + \int_{t_1}^{t_2} \delta W_{nc}\mathrm{d}t = 0 \tag{7}$$

where T is the total kinetic energy of the system, U the potential energy of deformation of the system and δW_{nc} the virtual work of the non-conservative forces acting in the system, between time interval t_1 to t_2.

The kinetic energy T of a plate, is given by (Meirovitch, 1986):

$$T = \frac{1}{2}\int \rho\{\dot{q}\}^T\{\dot{q}\}\mathrm{d}V \tag{8}$$

where V is the volume of the plate, ρ the mass density and $\{\dot{q}\}$ the generalized velocity vector.

For piezoelectric materials the electro-mechanical constitutive equations are coupled (Preumont, 1997), given by:

$$\begin{cases} \{\sigma\} = [C^E]\{\varepsilon\} - [e]\{E\} \\ \{D\} = [e]^T\{\varepsilon\} + [\xi^\varepsilon]\{E\} \\ [e] = [d][C^E] \end{cases} \tag{9}$$

where $\{\sigma\}$ is the stress vector, $[C^E]$ the stiffness matrix, $\{\varepsilon\}$ the mechanical strain vector, $[e]$ the piezoelectric coefficient matrix, $\{E\}$ the electric field vector, $\{D\}$ the electric charge density vector, $[\xi^\varepsilon]$ the dielectric constant at constant strain and $[d]$ the piezoelectric constant matrix.

The system total potential energy comes from the constitutive equations and includes the mechanical and electric potential energies (Marques and Nagamine, 2001), that is:

$$U = \frac{1}{2}\int [\{\varepsilon\}^T\{\sigma\} - \{E\}^T\{D\}]\mathrm{d}V \tag{10}$$

The total work of the applied external forces is given by:

$$W = \{q\}\{P_c\} + \int_V \{q\}\{P_b\}\mathrm{d}V + \int_{S_1} \{q\}\{F_S\}\mathrm{d}S_1 - \int_{S_1} \{\phi\}Q\mathrm{d}S_2 \tag{11}$$

where $\{P_c\}$ is the concentrated force vector, $\{P_b\}$ the body force vector over the volume V, $\{P_S\}$ the surface force vector applied to the area S_1, $\{q\}$ the generalized displacement vector, $\{\phi\}$ the electric potential vector and Q the electric charge over the surface S_2.

Substituting Eqs. (8), (10) and (11) into equation Eq. (7), yields the variational equation, which is used to obtain the FE model, that is:

$$\begin{aligned} \textstyle\int_V [\rho\delta\{\dot{q}\}^T\{\dot{q}\} - \delta\{\varepsilon\}^T[C^E]\{\varepsilon\} + \delta\{\varepsilon\}^T[e]\{E\} - \delta\{E\}^T[\xi^\varepsilon]\{E\} + \delta\{q\}^T\{P_b\}]\mathrm{d}V \\ + \textstyle\int_{S_1} \delta\{q\}^T\{F_S\}\mathrm{d}S_1 + \delta\{q\}^T\{P_c\} - \int_{S_1} \{\phi\}Q\mathrm{d}S_2 = 0 \end{aligned} \tag{12}$$

2.3.2 Active plate via finite element method

The linear model in finite elements of the structure considering plate element was based on the Kirchhoff's hypothesis and the electromechanical variacional principle for piezoelectric behavior (Lima, 1999). On the field of tensions, this model uses the rectangular element of Melosh, with three mechanical degrees of freedom per node, being displacements u, v and w at axies x, y and x, and an electric degree of freedom ϕ that depends on amount applied potential in the element. Fig. 2 illustrates this element with piezoelectric bonded in the two faces of the main structure (plate), where a, b and θ respectively represent the length, width and rotation of the faces, and h and h_{pe} are the thicknesses of the plate and and the piezoelectric ones.

Being the displacement on the neutral plan of the plate, where distance between to the neutral axis is z, as it shows in the Fig. 3, the nodal displacements are given by the following kinematic relations:

$$\begin{cases} u = -z\dfrac{\partial w}{\partial x} \\ v = -z\dfrac{\partial w}{\partial y} \\ w = w(x,y) \end{cases} \tag{13}$$

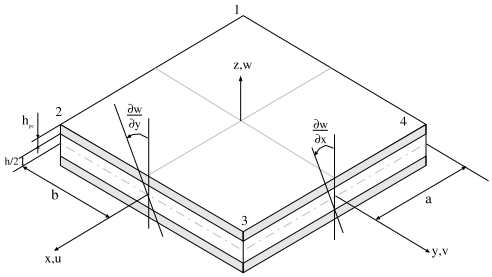

Figure 2. DOF of plate finite element with piezoelectric effect.

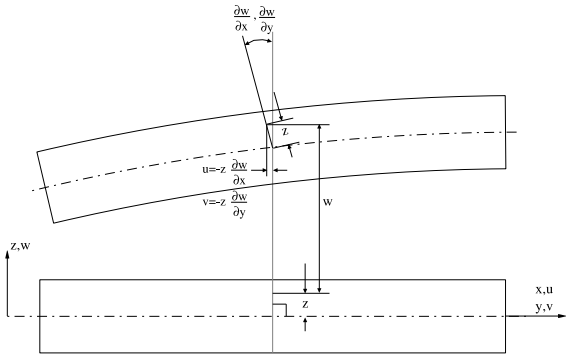

Figure 3. Plate displacement on the neutral axis.

For this element it is necessary to use a function from polynomial interpolation with 12 parameters, that is:

$$w|_{x_i,y_i} = d_1 + d_2x + d_3y + d_4x^2 + d_5xy + d_6y^2 + d_7x^3 + d_8x^2y + d_9xy^2 + d_{10}y^3 + d_{11}dx^3y + d_{12}xy^3 \quad (14)$$

Writing w in the matrix form, it goes:

$$w = \{P\}^T\{d\} \quad (15)$$

According to Eq. (13) and Eq. (14), in the matrix forms, the generalized coordinate vector can be writen as:

$$\{q\} = [X]\{d\} \quad (16)$$

where $[X]$ is:

$$[X] = \sum_{i=1}^{4} \begin{bmatrix} P(x_i, y_i) \\ \dfrac{\partial P(x_i, y_i)}{\partial x_i} \\ -\dfrac{\partial P(x_i, y_i)}{\partial y_i} \end{bmatrix} \quad (17)$$

Be $[Q_v]$ according to (Zienkiewicz and Taylor, 2000):

$$[Q_v] = \begin{bmatrix} \dfrac{\partial P}{\partial x} & \dfrac{\partial P}{\partial y} & P \end{bmatrix}^T \quad (18)$$

Inverting the transformation matrix $[X]$ and substituting in Eq. (16) it results in the following matrix:

$$[B_v] = [Q_v][X]^{-1} \quad (19)$$

where Eq. (13) can be represented in the following matrix form:

$$\{q\} = [Z][B_v]\{q_k\} \quad (20)$$

with:

$$[Z] = \begin{bmatrix} -z & 0 & 0 \\ 0 & -z & 0 \\ 0 & 0 & 1 \end{bmatrix} \quad (21)$$

According to Fig. 2, the coordinates x and y, for nodes $i = 1...4$, are: $(x_1, y_1) = (-a, -b)$, $(x_2, y_2) = (a, -b)$, $(x_3, y_3) = (a, b)$ and $(x_4, y_4) = (-a, b)$.

The nodal displacement relations for the plate element are given by:

$$\begin{cases} \varepsilon_x = \dfrac{\partial u}{\partial x} = -z\dfrac{\partial^2 w}{\partial x^2} \\ \varepsilon_y = \dfrac{\partial v}{\partial y} = -z\dfrac{\partial^2 w}{\partial y^2} \\ \Upsilon_{xy} = \dfrac{\partial u}{\partial y} + \dfrac{\partial v}{\partial x} = -2z\dfrac{\partial^2 w}{\partial x \partial y} \end{cases} \quad (22)$$

By Eqs. (22) and (15) it follows:

$$[Q_k] = \left[\begin{array}{ccc} \dfrac{\partial^2 P}{\partial x^2} & \dfrac{\partial^2 P}{\partial y^2} & 2\dfrac{\partial^2 P}{\partial x \partial y} \end{array} \right]^T \tag{23}$$

that substituing in the Eq. (16) results on the matrix:

$$[B_k] = [Q_k][X]^{-1} \tag{24}$$

Being, thus, the Eq. (22) can be represented in the following matrix form:

$$\{\varepsilon\} = -z[B_k]\{q\} \tag{25}$$

Potential energy

From Eq. (12), the potential energy of the main structural element (V_{st} domain, that is, integration defined over the intervals $x = [-a; a]$, $y = [-b; b]$ and $z = [-h/2; h/2]$), is obtained by:

$$\delta U_{st} = \int_{V_{st}} \delta\{\varepsilon\}^T \{\sigma\} \mathrm{d}V = \int_{V_{st}} \delta\{\varepsilon\}^T [C_{st}^E]\{\varepsilon\} \mathrm{d}V \tag{26}$$

where $[C_{st}^E]$ is the element constitutive equations given on matrix form by:

$$[C_{st}^E] = \frac{E_{st} h_{st}}{1 - \mu_{st}^2} \left[\begin{array}{ccc} 1 & \mu_{st} & 0 \\ \mu_{st} & 1 & 0 \\ 0 & 0 & \dfrac{1 - \mu_{st}}{2} \end{array} \right] \tag{27}$$

where E_{st} is the Young's modulus and μ_{st} is the coefficient of Poisson of the main structure.

Substituing Eq. (24) in Eq. (26), it follows:

$$\delta U_{st} = \{\delta q\}^T \int_{V_{st}} [B_k]^T [Z]^T [C_{st}^E][B_k] \mathrm{d}V \{\delta q\} \tag{28}$$

where the stiffness strutural matrix can be represented by:

$$[k_{qq_{st}}] = \int_{V_{st}} [B_k]^T [Z]^T [C_{st}^E][B_k] \mathrm{d}V \tag{29}$$

The elasticity piezoelectric modulus E_{pe}, the coefficient of Poisson μ_{pe} and the constitutive equation of the piezoelectric element, then, in the same way that it was made to get the stiffness matrix of the main structure, the piezoelectric stiffness matrix is:

$$[k_{qq_{pe}}] = \int_{V_{pe}} [B_k]^T [Z]^T [C_{pe}^E][B_k] \mathrm{d}V \tag{30}$$

where the integration domain of the volume V_{pe} defined over the volumes of the piezoelectric elements, that is, the intervals $x = [-a; a]$, $y = [-b; b]$ and $z = [-h_{pe} - h/2; -h/2]$ for piezoelectric below the main structure and $z = [h/2; h/2 + h_{pe}]$ for the piezoelectric one above.

The electro-mechanical stiffness matrices are given by:

$$[k_{q\phi}] = \int_{V_{pe}} [B_k]^T [Z]^T [e][B_\phi] \mathrm{d}V \tag{31}$$

$$[k_{\phi q}] = [k_{q\phi}]^T \tag{32}$$

where:

$$[B_\phi] = \left[\begin{array}{cc} \dfrac{1}{h_{pe}} & 0 \\ 0 & \dfrac{1}{h_{pe}} \end{array} \right] \tag{33}$$

The dielectric rigidity matrix is given by:

$$[k_{\phi\phi}] = \int_{V_{pe}} [B_\phi]^T [\xi^\varepsilon][B_\phi] \mathrm{d}V \tag{34}$$

Kinetic energy

To calculate the term of kinetic energy of Eq. (8), considers Eq. (20), resulting in the following expression:

$$\delta T = \int_V \rho_V \{\dot{q}\}^T [B_v]^T [Z]^T [Z][B_v]\{\dot{q}\} \mathrm{d}V \tag{35}$$

where the mass matrix on volume V enclosing the main V_{st} and the piezoelectric V_{pe} volumes, is obtained as:

$$[m] = \int_V \rho_V [B_v]^T [Z]^T [Z][B_v] \mathrm{d}V \tag{36}$$

Virtual work of the forces and external loads

In accordance with the term of the virtual work done by the forces and external loads of the Eq. (12), and considering Eq. (20), the virtual work of the external forces vector $\{f_s\}$ is:

$$\delta W = \delta\{q\}^T \int_A [B_v]^T \{f_s\} \mathrm{d}A \tag{37}$$

where:

$$\{F_s\} = \int_A [B_v]^T \{f_s\} \mathrm{d}A \tag{38}$$

Global system equations

Substituting the kinetic energy equations, potential of deformation and work of the external forces in the electromechanical variational principle equation and considering the equilibrium for finite elements, one can yield the global dynamic equations of the system:

$$[M_{qq}]\{\ddot{q}\} + [K_{qq}]\{q\} = \{F_s\} - [K_{q\phi a}]\{\phi\} \tag{39}$$

where $[M_{qq}]$, $[K_{qq}]$, $[K_{q\phi a}]$ are the mass, stiffness and electro-mechanical matrices, and $\{F_s\}$ and $\{\phi\}$ are external mechanical and electric loading vectors.

3. VORTEX LATTICE METHOD

The VLM consists of distributing plane vortex singularities over a lifting surface and its wake (Katz and Plotkin, 1991). The plane vortex singularities satisfy the Laplace equation and when it is combined with the uniform stream incompressible and potential flows around the wing the aerodynamic loading can be calculated. Here, to implement the VLM, the wing has been represented by a lifting surface without thickness and discretized in quadrilateral elements (panels). A vortex ring is associated with each panel, being the leading segment of each vortex ring placed on the panel quarter chord line and its control point placed at the center of the three-quarter chord line. The wing discretization scheme is shown in Fig. 4. To guarantee that the flow streamlines pass over the lifting surface, it is necessary to satisfy the boundary condition of zero normal velocity on the wing surface. This boundary condition is applied at the control points and it results in the correct values for the vortex singularities (circulation Γ).

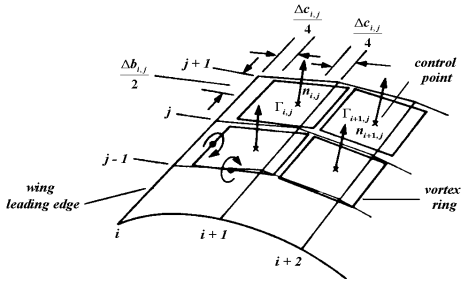

Figure 4. Wing discretization scheme (Katz and Plotkin, 1991).

The boundary condition in each panel can be expressed as

$$(\nabla\phi + v_m + v_w) \cdot \{n\} = 0 \tag{40}$$

where the gradient of the potential velocity ϕ corresponds to the perturbed velocities induced by the wing vortex singularities, v_m corresponds to the velocity of the wing motion (the freestream velocity relative to the wing plus the velocities of the wing structural deformations), v_w corresponds to the velocities induced by the wake, and n is the normal vector.

The velocity V induced by each straight vortex segment, extending from point 1 to point 2, at an arbitrary point P, obeys the Biot-Savart law, that is:

$$V = \frac{\Gamma}{4\pi}\frac{r_1 \times r_2}{|r_1 \times r_2|^2}(r_1 - r_2)\cdot\left(\frac{r_1}{|r_1|} - \frac{r_2}{|r_2|}\right) \tag{41}$$

where, r_1 and r_2 are the vectors that define the position of point P in relation to the points 1 and 2.

It is important to note that the value of the circulation Γ is still not known in Eq. (41). So, only the values of the other terms will be calculated. This is done by assuming $\Gamma = 1$. The velocity induced by each vortex ring at a point P is obtained adding the results obtained with Eq. (41) for the four corresponding vortex segments. The velocity is referred as the velocity induced by the vortex ring L on the control point K. Applying the zero normal velocity boundary condition at the control point $K = 1$,

$$(V_1 1\Gamma_1 + V_1 2\Gamma_2 + V_1 3\Gamma_3 + \ldots + V_1 m\Gamma_m + v_m 1 + v_w 1)\cdot n_1 = 0 \tag{42}$$

where the circulations in each vortex ring are the unknowns and m is the number of panels used in the wing aerodynamic discretization.

Based on Eq. (42), the so-called influence coefficients ($a_{KL} = V_{KL}\cdot n_k$) can be defined. Re-writing this equation as a function of the influence coefficients for each of the m control points and passing v_m and v_w to the right-hand side (RHS) of the equation, the following linear system is obtained:

$$\begin{bmatrix} a_{11} & a_{12} & \cdots & a_{1m} \\ a_{21} & a_{22} & \cdots & a_{2m} \\ \vdots & \vdots & \ddots & \vdots \\ a_{m1} & a_{m2} & \cdots & a_{mm} \end{bmatrix} \begin{Bmatrix} \Gamma_1 \\ \Gamma_2 \\ \vdots \\ \Gamma_m \end{Bmatrix} = - \begin{Bmatrix} v_{m1} + v_{w1} \\ v_{m2} + v_{w2} \\ \vdots \\ v_{mm} + v_{wm} \end{Bmatrix} \cdot \begin{Bmatrix} n_1 \\ n_2 \\ \vdots \\ n_m \end{Bmatrix} \tag{43}$$

The evaluation of v_m consists of two steps: 1) the freestream velocity is obtained moving the wing in the aft direction, and 2) the velocities of the structural deformations are obtained solving the equation of motion (Eq. (6)). The velocities induced by the wake (v_w vector) are obtained employing the Biot-Savart law (Eq. (41)). It is important to consider that a portion of the wake is generated at each time interval, according to Fig. 5. The circulation values of the last vortex rings generated are the same as those of the trailing edge vortex rings, to satisfy the three-dimensional Kutta condition. Thus, at each time interval new vortex rings are generated and the corresponding values of circulation are found. The value of circulation of each wake vortex ring remains the same during all the simulation time. In the present simulation, the wake rollup has not been considered, so the wake is parallel to the freestream velocity plane.

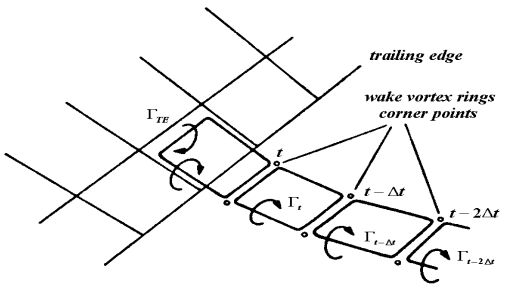

Figure 5. Wake discretization scheme (Katz and Plotkin, 1991).

The solution of the linear system given by Eq. (43) provides the circulation values for the wing vortex rings, which has been employed for the aerodynamic loads calculation. The unsteady Bernoulli equation for each panel is:

$$\frac{p_l - p_u}{\rho} = \frac{V_u^2}{2} - \frac{V_l^2}{2} + \frac{\partial\phi_u}{\partial t} - \frac{\partial\phi_l}{\partial t} \tag{44}$$

where p is the static pressure and the subscripts u and l refer to the upper and lower sides of the panel.

The last two terms in Eq. (44) refer to the unsteady case. The difference between them is obtained from the definition of circulation (Katz and Plotkin, 1991), that is:

$$\frac{\partial\phi_u}{\partial t} - \frac{\partial\phi_l}{\partial t} = \frac{\partial(\phi_u - \phi_l)}{\partial t} = \frac{\partial\Gamma}{\partial t} = \frac{\Gamma(t) - \Gamma(t-1)}{\Delta t} \tag{45}$$

If $\partial\Gamma/\partial t = 0$, Eq. (44) is analogous to the classical Bernoulli equation for the steady case, and the first two terms can be determined with the aid of the Kutta-Joukowski theorem, that is:

$$\frac{V_u^2}{2} - \frac{V_l^2}{2} = \frac{V_\infty \Gamma \Delta b cos\alpha}{S} \tag{46}$$

where V_∞ is the free stream velocity, α is the local angle of attack, Δb is the length of the panel in the spanwise direction and S is the panel area.

Substituting Eqs. (45) and (46) into Eq. (44), the normal force in each panel can be computed and supplied as input to the equation of motion (Eq. (6)). It is important to emphasize that the values of Γ in the above equations are given by $\Gamma_{i,j}$ for the wing leading edge panels, and by $(\Gamma_{i,j} - \Gamma_{i-1,j})$ for the other panels (Benini, 2002).

4. ACTIVE CONTROL VIA FUZZY LOGIC

The FL controller for suppressing undesired aeroelastic response on a smart wing has been based on the Mamdani-type fuzzy model (Yager and Filev, 1994). A decision surface has been obtained from error measurements based on structural vibrations to be cancelled, and control action in terms of voltage variations to the piezoelectric actuators. The decision surface represents, therefore, the control law on unitary discourse universe. Here, the control law models the consequent control action like a PD-type control. The error signal comes from the difference between the wing tip displacement and a reference value (here, it has been adopted as zero). The input and output signals are normalized by individual gains. These gains are obtained manually and they guarantee stable and efficient response control. The fuzzy membership functions are also obtained and tuned manually. Tab. 1 shows the rule basis and Fig. 6 shows the respective decision surface. The controller gains tuned manually are $k_e = 133m^{-1}$, $k_{\Delta e} = 341(m/s)^{-1}$ and $k_u = 872V^{-1}$.

To enhance control actions, the decision surface has been interpolated using an ANN, in order to speed up the system simulation (Souza et al., 2002). The ANN under consideration is a feed-forward neural network with four layers: 2 inputs (error and change of error signals), 2 hidden layers with 20 and 10 neurons, respectively, and one output (control action). The neurons activation functions are all sigmoid ones and the ANN has been trained with a back-propagation algorithm. Figure 7 shows the closed loop to control de aeroelastic problem. The required control actions when using the FC can be gotten now using it ANN, which represents with exactness the same decision surface of FC.

Table 1. Rule basis of the FL controller.

$e \diagdown \Delta e$	NG	NP	Z	PP	PG
NG	NG	NG	NP	NP	Z
NP	NG	NG	NP	Z	PP
Z	NP	Z	Z	Z	PP
PP	NP	Z	PP	PG	PG
PG	Z	PP	PP	PG	PG

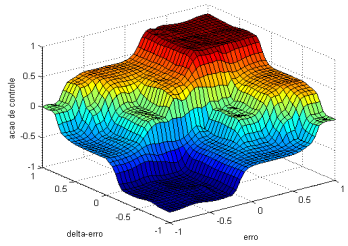

Figure 6. Decision surface of the FL controller.

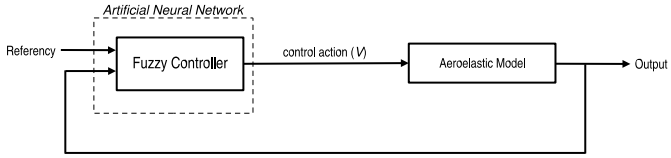

Figure 7. Smart wing aeroelastic control driagram.

5. RESULTS

Some results of a linear flexible wing structure with $0.8m$ semi-span and $0.25m$ chord are showed on Fig. 8 to 10, with open-loop and closed-loop results. For structural model a 30×5 Kirchhoff plate finite elements are considered. For the aerodinamic mesh 8 longitudinal and 4 transversal panels are adopted. The velocity of the free stream is $30\frac{m}{s}$. It is used four pairs of hypothetical piezoelectric actuators, one above and other below of the main structure, distributed throughout along the semi-span. The control signal is activated after $0.1s$, for the control of the tip wing vertical displacement. One can note the suppression of vertical vibration of wing tip mid-chord reflecting on suppression of the first mode, as can be

noticed on frequency response of vertical displacement. It can also be noted the piezoelectric input voltage, that can be considered for optimization of the controller and minimising the cost of physical implementation.

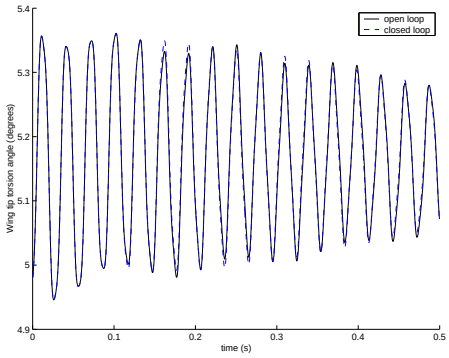

Figure 8. Wing tip torsion angle for $V_\infty = 30\frac{m}{s}$.

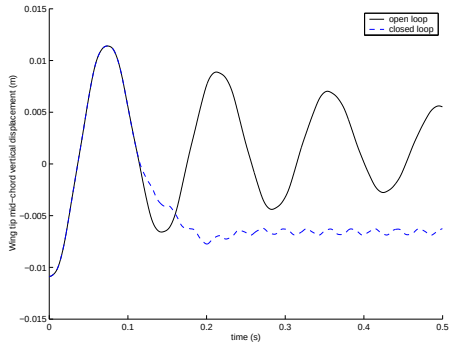

Figure 9. Wing tip vertical displacement for $V_\infty = 30\frac{m}{s}$.

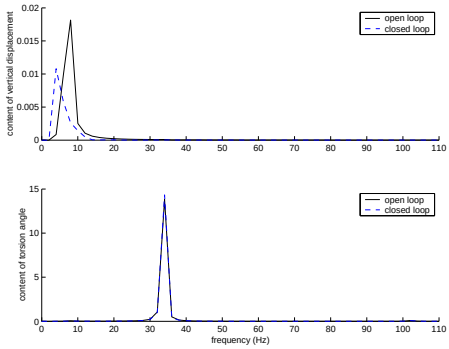

Figure 10. Response frequency for $V_\infty = 30\frac{m}{s}$.

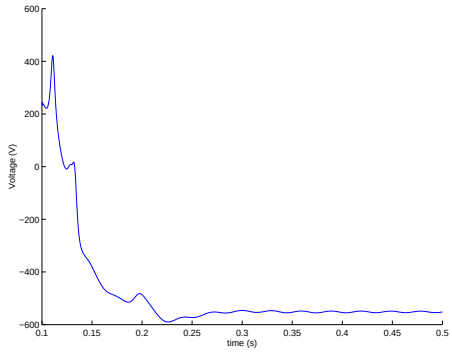

Figure 11. Voltage applied to the piezoelectric actuators set.

Active control performance has also been verified for free stream velocity of $140\frac{m}{s}$, as showed on Fig. 12 to 14. One can observe an instability on open-loop, characterizing the flutter phenomena. The control signal is activated after $0.1s$, for the control of the wing tip mid-chord displacement. It can also be noticed the vibration suppression, despite the flutter occurrrence. Although the control action is for suppression of the first mode, the attenuation occurs on second flexural and first torsional modes, as showed on Fig. 14, noticing the coupling of these modes, characterizing the flutter phenomena. It's because the position and dimensions of the actuators along the structure. However, the control action on piezoelectric actuators for flutter suppression are excessively high comparing with the previous case. This means that in practical terms this control is very expensive.

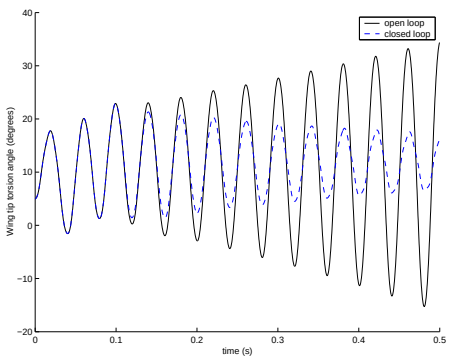

Figure 12. Wing tip torsion angle for $V_\infty = 140\frac{m}{s}$.

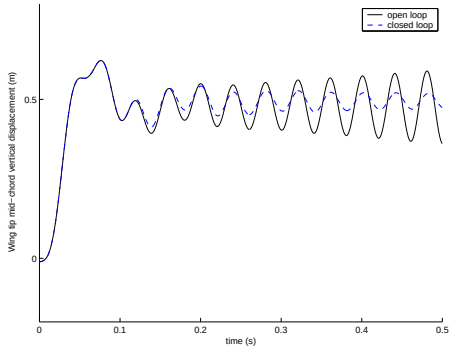

Figure 13. Wing tip vertical displacement for $V_\infty = 140\frac{m}{s}$.

6. CONCLUDING REMARKS

As it can be seen, the results of controlling the linear flexible wing structure are satisfactory, showing the suppression of vertical vibration of the wing, reflecting on suppression of vibration of the first mode. It can be seen too, that for flutter

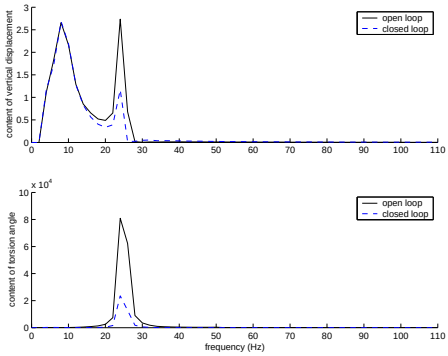

Figure 14. Response frequency for $V_\infty = 140\frac{m}{s}$.

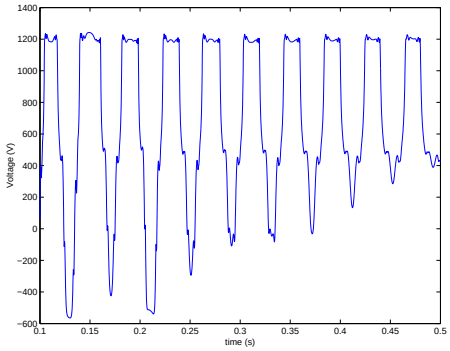

Figure 15. Voltage applied to piezoelectric actuators set.

phenomenon control it is satisfactory, but represents an expensive practical control to apply in aircraft, because the high voltages required, despite the piezoelectric actuators being hypothetical.

The non-linearity by large displacement will be included in aeroelastic control of smart wing in the next step.

7. ACKNOWLEDGEMENTS

The authors acknowledge the financial support of CAPES (33002045011/M8) during the tenure of this research work.

8. REFERENCES

Benini, G. R. and Belo, E. M., 2001, "The vortex lattice method for unsteady aerodynamics", Proceedings of the 16th Brazilian Congress of Mechanical Engineering.

Benini, G. R., 2002, "Numerical model for aeroelastic response simulation of fixed wings", Master Thesis, University of São Paulo, São Carlos, SP, Brazil (in Portuguese).

Cesnik, C. E. S. and Brown, E. L., 2002, "Modeling of high aspect ratio active flexible wings for roll control", Proceedings of the 43th AIAA, Structures, Structural Dynamics and Materials Conference.

Crawley, E. F., 1994, "Intelligent structures for aerospace: a technology overview and assessment", AIAA Journal, 32(8):1689-1699.

Dowell, E. H. and Tang, D., 2002, "Nonlinear aeroelasticity and unsteady aerodynamics", AIAA Journal, 40(9):1697-1707.

Forster, E. and Livne, E., 2000, "Integrated structure actuation synthesis of strain actuated devices for shape control", Proceedings of the 42nd AIAA, Structures, Structural Dynamics and Materials Conference.

Gern, F. H., Inman, D. J. and Kapania, R. K., 2001, "Structural and aeroelastic modeling of general planform UCAV wings with morphing airfoils", AIAA 2001-1369.

Gruppioni, E. M., 2003, "Parameter optimization of fuzzy controllers for smart structures", Master Thesis, University of São Paulo, São Carlos, SP, Brazil (in Portuguese).

Haykin, S., 1999, "Neural networks: a comprehensive foundation", 2. ed. Upper Saddle River, N.J.: Prentice Hall.

Katz, J. and Plotkin, A., 1991, "Low-speed aerodynamics: from wing theory to panel methods", New York: McGraw-Hill.

Lima Jr., J. J., 1999, "Modeling of piezoeletric sensors and actuators with applications in active control of structures, Ph. D. Thesis, Faculdade de Engenharia Mecânica, Universidade Estadual de Campinas (in Portuguese).

Marques, F. D. and Nagamine, R. K., 2001, "Non-conventional control approach for intelligent structures", In: AIAA/ ASME/ ASCE/ AHS/ ASC Structures, Struc. Dynamics, And Materials Conf. And Exhibit, 42. AIAA 2001-1683.

Meirovitch, L., 1986, "Elements of Vibration Analysis", New York: McGraw-Hill.

Nagamine, R. K., 2001, "Fuzzy logic for non-conventional control of an intelligent beam", Master Thesis, University of São Paulo, São Carlos, SP, Brazil (in Portuguese).

Patil, M. J., Hodges, D. H. and Cesnik, C. E. S., 2001, "Nonlinear aeroelasticity and flight dynamics of high-altitude long-endurance aircraft", Journal of Aircraft, 38(1):88-94.

Souza, L. F. R., Gruppioni, E. M., Belo, E. M. and Marques, F. D., 2002, "Identificação da dinâmica não linear de uma pá de helicóptero via redes neurais", Proceedings of the 2nd National Congress of Mechanical Engineering, João Pessoa.

Yager, R. R. and Filev, D. P., 1994, "Essentials of fuzzy modeling and control", John Wiley and Sons, New York.

Zienkiewicz, O. C. and Taylor, R. L., 2000, "The finite element method. Volume 2: Solid Mechanics", Oxford: Butterworth-Heinemann.

9. Responsibility notice

The authors are the only responsible for the printed material included in this paper.